Vapor-Liquid-Solid Growth and Optoelectronics of Gallium Sulfide van der Waals Nanowires

Eli Sutter,[1,*] Jacob S. French,[2] Stephan Sutter,[2] Juan Carlos Idrobo,[3] and Peter Sutter[2,*]

[1]Department of Mechanical & Materials Engineering, University of Nebraska-Lincoln, Lincoln, Nebraska 68588, USA

[2]Department of Electrical & Computer Engineering, University of Nebraska-Lincoln, Lincoln, Nebraska 68588, USA

[3]Center for Nanophase Materials Sciences, Oak Ridge National Laboratory, Oak Ridge, TN 37831, United States

Abstract

Nanowires of layered van der Waals (vdW) crystals are of interest due to structural characteristics and emerging properties that have no equivalent in conventional 3D crystalline nanostructures. Here, vapor-liquid-solid growth, optoelectronics, and photonics of GaS vdW nanowires are studied. Electron microscopy and diffraction demonstrate the formation of high-quality layered nanostructures with different vdW layer orientation. GaS nanowires with vdW stacking perpendicular to the wire axis have ribbon-like morphologies with lengths up to 100 micrometers and uniform width. Wires with axial layer stacking show tapered morphologies and a corrugated surface due to twinning between successive few-layer GaS sheets. Layered GaS nanowires are excellent wide-bandgap optoelectronic materials with E_g = 2.65 eV determined by single-nanowire absorption measurements. Nanometer-scale spectroscopy on individual nanowires shows intense blue band-edge luminescence along with longer wavelength emissions due to transitions between gap states, and photonic properties such as interference of confined waveguide modes propagating within the nanowires. The combined results show promise for applications in electronics, optoelectronics and photonics, as well as photo- or electrocatalysis owing to a high density of reactive edge sites, and intercalation-type energy storage benefitting from facile access to the interlayer vdW gaps.

Keywords: nanowires, layered crystals, semiconductors, optoelectronics, photonics

*Corresponding authors, e-mail: psutter@unl.edu; esutter@unl.edu

One-dimensional (1D) nanowires of 2D layered crystals hold promise for opening up tunable structural, optoelectronic, electronic transport and device characteristics. Nanowires of 2D materials show structural characteristics and emerging properties that have no equivalent in nanowires of conventional 3D crystals. For example, a layered nanowire can crystallize with its van der Waals layers stacked parallel or perpendicular to the wire axis, leading to potentially very different properties in charge transport or optoelectronics due to the anisotropy imposed by in-plane covalent and interlayer van der Waals bonding. Even phenomena that are well established for 3D-crystalline nanowires can lead to distinct effects. In van der Waals nanowires with layers stacked along the wire axis, for instance, Eshelby twist due to an axial screw dislocation can give rise to a chiral structure with diameter-controlled interlayer twist, harboring size-tunable twist moiré patterns and associated modulations of the optoelectronic properties.[1] Nanowires of layered van der Waals crystals have been demonstrated for several materials, including GeS,[1-3] MoS_2,[4] GaSe,[5] InSe, and GeSe. Here, we discuss the vapor-liquid-solid (VLS) growth, optoelectronics, and photonics of GaS van der Waals nanowires.

Group III monochalcogenides – and GaS in particular – are layered semiconductors whose basic building blocks comprise a double layer of metal atoms (rather than the usual single metal layer, as in the transition metal dichalcogenides)[6] sandwiched between layers of chalcogen atoms, *i.e.*, a GaS monolayer contains four planes of gallium and sulfur atoms stacked along the *c*-axis in the sequence S–Ga–Ga–S. The bonding within each layer is predominantly covalent/ionic whereas adjacent layers, stacked along the *c*-axis, are held together by weak dispersion forces. GaS nanosheets have attracted attention due to their promise for diverse applications that could benefit from their chemical, electronic, and optoelectronic properties. Specific areas of interest include hydrogen evolution catalysis,[7] optoelectronics and high-performance photodetectors,[8]

heterostructure UV photodetectors[9] and detectors operating in different gas environments,[10] flexible and transparent transistors and gas sensors,[11] as well as mechanical applications benefiting from a high Young modulus of GaS comparable to that of WS_2.[12] Theoretical calculations indicate that the electronic properties of GaS layers are sensitive to strain and electric fields,[13] with strain causing a transition from a trivial to a topological insulator.[14] Strained states could be achieved through embedding in various heterostructures, *e.g.*, ZrS_2/GaS[15] or arsenene/GaS.[16] Of fundamental interest is the appearance of an electron-hole liquid condensate state[17] at elevated temperature $T = 130$ K in bulk GaS.[18] Similar to MoS_2,[19,20] SnS_2,[21] and WS_2,[22] GaS sheets roll easily to form nanotubes.[23,24] Other 1D nanostructures of GaS, such as nanohorns[25] and nanobelts,[26] have been demonstrated. While the nanobelts clearly show a ribbon-like stacking of GaS sheets with *c*-axis perpendicular to the axis of the 1D nanostructure, reported nanowires have so far not been sufficiently characterized for an unambiguous assignment of the crystal polymorph (*e.g.*, layered GaS *vs.* 3D-crystalline Ga_2S_3). In general, prior measurements of the properties of GaS nanostructures were limited to ensemble measurements such as photoluminescence (PL) spectroscopy, and an understanding of the individual optoelectronic and photonic properties of these nanostructures has not been developed. Here we establish the bottom-up synthesis of layered GaS van der Waals nanowires by a vapor-liquid-solid (VLS) process using Au and Ag nanoparticles as catalysts. (Scanning) transmission electron microscopy ((S)TEM) and electron diffraction are used to determine the structure and infer the growth mechanism of the nanowires. Advanced electron microscopy based spectroscopy methods with spatial resolution far below the diffraction limit, including optical absorption measurements by electron energy-loss spectroscopy (EELS) in monochromated STEM and light emission excited at the nanometer-scale in cathodoluminescence spectroscopy

(STEM-CL), are applied to establish the optoelectronic properties of individual layered GaS nanowires. The results demonstrate the formation of high-quality layered 1D nanostructures with different van der Waals stacking orientation – parallel or perpendicular to the wire axis – by VLS growth with Ag catalysts, whereas only one type of nanowire is observed for growth with Au catalysts. Nanowires with different layer orientation crystallize in different morphologies, straight ribbon-like or tapered with truncated triangular cross-section, explained by different wetting behaviors of the VLS catalyst and accumulation of Ga in the catalyst during growth. Electron-stimulated spectroscopy on single nanowires shows promising optoelectronic properties such as intense blue band-edge emission along with transitions between gap states that are characteristic for GaS. Sub-diffraction luminescence maps identify confined photonic waveguide modes propagating within the nanowires. The results establish the controlled synthesis of high-quality GaS van der Waals nanowires with potential applications in electronics, optoelectronics and photonics, as well as energy conversion and storage.

Results and Discussion

Vapor-Liquid-Solid Growth and Structure of GaS van der Waals Nanowires

GaS nanowires were grown in a reactor with two independently controlled temperature zones by thermal evaporation of GaS powder using Ar:H_2 (98:2) as a carrier gas (see Methods for details). SiO_2/Si substrates were covered by thin films of Ag or Au, which thermally dewet at the growth temperature[27] to generate polydisperse arrays of supported Ag or Au nanoparticles that served as the VLS growth catalysts.

Typical GaS nanowires grown at a substrate temperature (T_s) of 550-600°C using Ag catalysts on SiO_2/Si are shown in the scanning electron microscopy (SEM) image in **Figure 1** (a). The as-

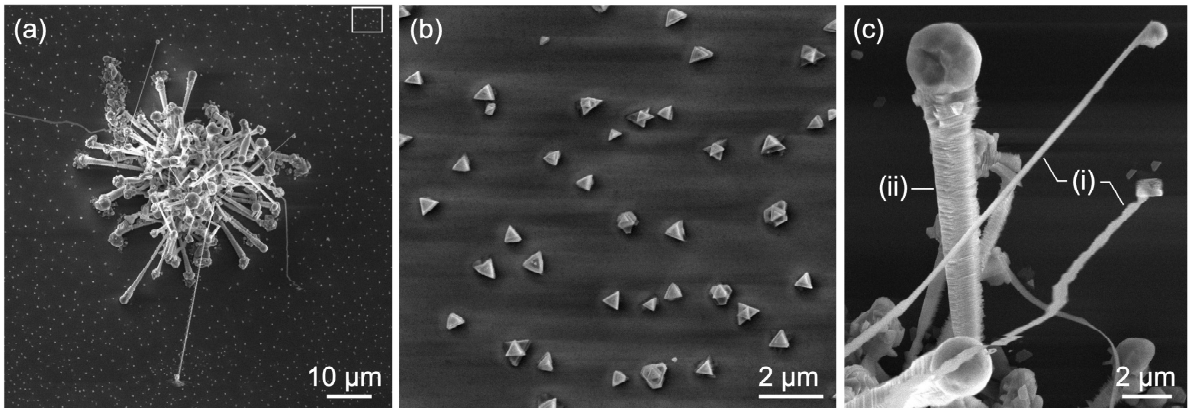

Figure 1. GaS nanowires on the growth substrate (Ag film on SiO_2/Si). (a) SEM image of a characteristic group of GaS nanowires on SiO_2/Si substrate covered with an Ag film with 2 nm nominal thickness (growth temperature T_s = 600°C). **(b)** Higher magnification SEM image of the area of the substrate away form the nanowires marked by a rectangle in (a). **(c)** Higher magnification SEM image of the GaS nanowires, showing two typical wire morphologies: thin ribbon-like wires with strongly protruding catalyst particles (type (i)), and thicker tapered nanowires with large catalyst particles at their tips (type (ii)).

grown nanowires usually form in isolated groups surrounded by areas in which the substrate is covered with planar triangular or truncated triangular flakes (Figure 1 (a), (b)). Analysis of SEM images shows typical areal densities of the 2D GaS flakes of (34 ± 6) flakes per 100 µm^2, except in denuded zones near groups of nanowires where the density is lower (Fig. 1 (a)). Groups of nanowires, typically 30 - 50 µm in diameter and containing several tens of nanowires, are separated by a few hundred µm on average under our growth conditions. The nanowires grow up to several tens of micrometers long, whereas the planar flakes reach typical side lengths of ~1 µm. Zoomed-in SEM images show the formation of two types of nanowires with different morphologies and diameters (Figure 1 (c)): Relatively narrow, straight or meandering wires with widths of ~100-200 nm carrying catalyst particles at their tips whose diameter is far larger than the footprint of the wire (type (i), Figure 1 (c)); and tapered nanowires consisting of clearly resolved layer stacks along their axis and whose diameters increase significantly along their

lengths (type (ii), Figure 1 (c)). The latter carry large spherical cap shaped catalyst particles at their tips, whose basal diameter matches the diameter of the adjacent wire.

We used (S)TEM imaging and electron diffraction to investigate the structure and morphology of the two types of VLS nanowires grown on Ag catalysts, including an unambiguous identification of the crystal polymorph as layered gallium (II) sulfide (GaS). The analysis of type (i) and type

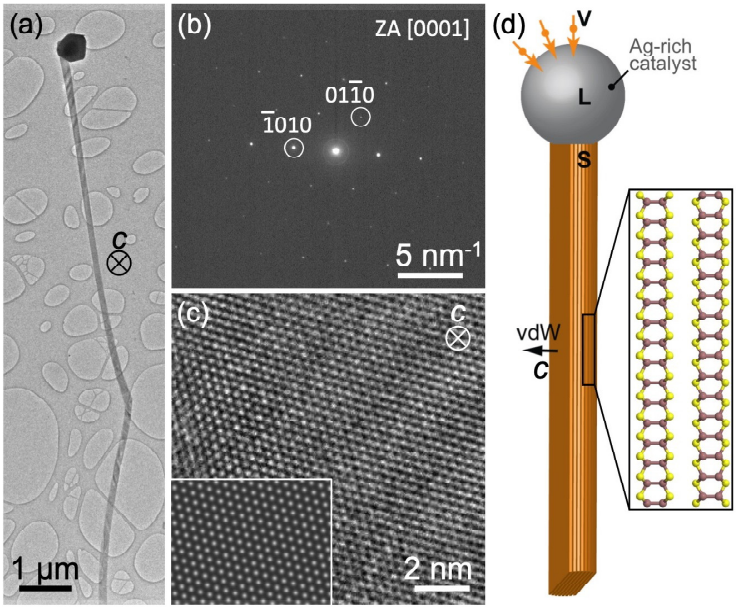

Figure 2. Ribbon-like GaS nanowires with *c*-axis (vdW) perpendicular to the nanowire axis, grown using Ag catalysts. (a) TEM image of a GaS nanowire transferred to amorphous carbon film (growth temperature T_s = 600°C). The GaS *c*-axis is perpendicular to the plane of the image, as indicated. **(b)** Diffraction pattern of the GaS nanowire. Zone axis (ZA): [0001]. **(c)** High-resolution TEM image of the GaS nanowire. Inset: Multislice image simulation. **(d)** Schematic representation of the layered structure of the ribbon-like GaS nanowire.

(ii) wires is summarized in Figure 2 and Figure 3, respectively. TEM imaging of dry-transferred wires on amorphous carbon supports illustrates the high aspect ratio and constant diameter over extended distances of type (i) nanowires (**Figure 2** (a)), which can reach lengths approaching 100 µm. Selected-area electron diffraction (Figure 2 (b)) confirms that these wires consist of monocrystalline layered β-GaS (hexagonal, space group $P6_3/mmc$, a = 3.587 Å, c = 15.492 Å).[28] High-resolution TEM imaging (Figure 2 (c)) shows the characteristic atomic structure of the GaS

basal plane. The basal-plane imaging (zone axis, ZA: [0001]) implies that the *c*-axis (*i.e.*, the van der Waals stacking direction) of type (i) nanowires is perpendicular to the wire axis (Figure 2 (d)), similar – albeit much smaller in width and thickness – to GaS and GaSe ribbons reported earlier.[5,26] We refer to these type (i) nanostructures as ribbon-like GaS nanowires, which can be ultrathin, often as thin as a few monolayers as shown by additional TEM analysis (Figure S1). High-resolution TEM analysis (Fig. 2 (a), (c)) shows that the symmetry axis of these ribbon-like nanowires is oriented along the [010] crystallographic direction (or $[\bar{1}\,2\,\bar{1}\,0]$ in four-index notation).

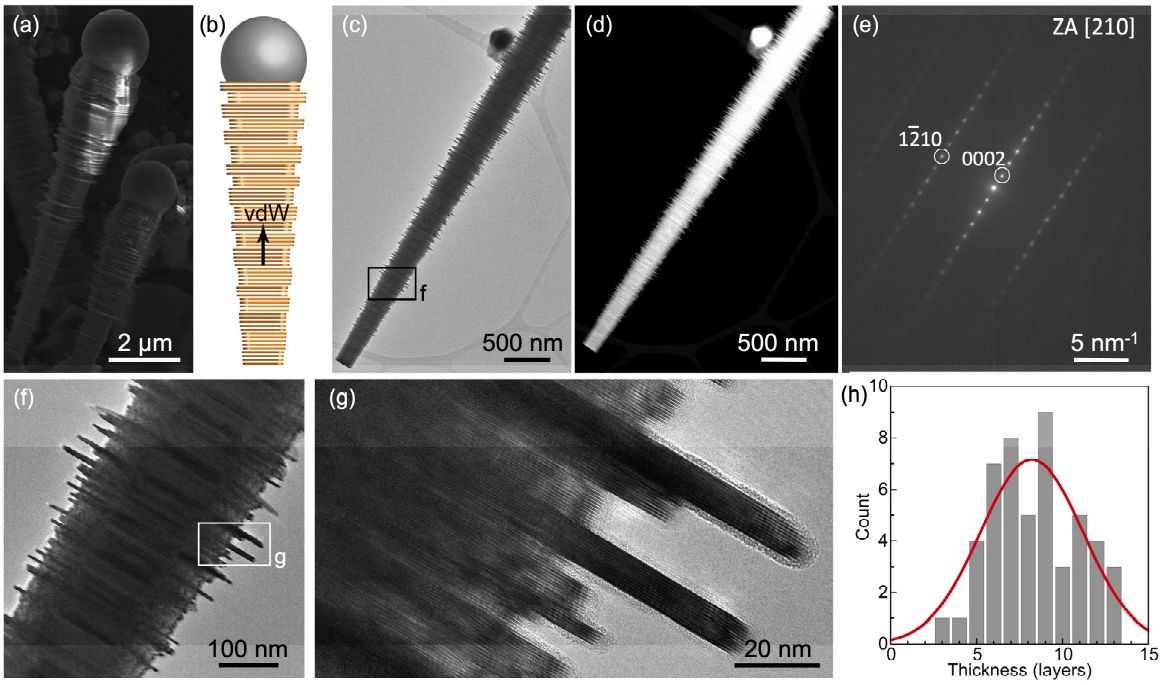

Figure 3. Tapered type (ii) GaS nanowires with *c*-axis (vdW) parallel to the nanowire axis, grown using Ag catalysts. (a) SEM image of GaS nanowires showing a tapered shape with increasing diameter toward the catalyst particles at the tips. **(b)** Schematic representation of the layered GaS nanowire. **(c)-(d)** TEM and HAADF-STEM images of a GaS nanowire transferred to amorphous carbon film (growth temperature T_s = 600°C). **(e)** Electron diffraction pattern of the GaS nanowire shown in (c), (d). Zone axis (ZA): [210]. **(f)** Higher magnification TEM image of the section of the GaS nanowire marked by a rectangle in (c). **(g)** High-resolution TEM image of the area marked in (f). **(h)** Thickness distribution of the protruding GaS layers at the sides of type (ii) nanowires, obtained from an analysis of high-resolution TEM lattice images. Red line: Gaussian fit to the data with a mean thickness of 8.2 layers.

Similar to these results with Ag catalysts, Au-catalyzed VLS growth can also produce ribbon-like GaS nanowires. GaS deposition on Au covered SiO_2/Si substrates across a wide range of substrate temperatures (450°C ≤ T_s ≤ 650°C) invariably results in the predominant formation of GaS flakes (Figure S2) and a smaller amount of ribbon-like GaS nanowires (Figure S3). The ribbon-like nanowires again grow with the GaS *c*-axis (*i.e.*, van der Waals stacking) perpendicular to the wire axis. However, they are usually not straight but have a characteristic meandering zigzag morphology[26] with non-uniform width that decreases towards the tip. The tip itself is identified by a small Au particle (dark in TEM, Figure S3 (a); bright in STEM, Figure S3 (b)). Importantly, for GaS growth on Au only the ribbon-like type (i) nanowires were observed under all growth conditions. Other wire morphologies, such as the type (ii) wires grown with Ag catalysts, were not found.

Type (ii) nanowires grown with Ag VLS catalysts have a very different morphology from the straight, ribbon-like type (i) GaS wires (**Figure 3**). SEM images (Figure 3 (a)) generally show large particles at their tips, a tapered shape with increasing diameter from root to tip, and surfaces that are not smooth but typically consist of clearly discernible stacks of sheets (Figure 3 (b)). (S)TEM imaging illustrates the uniformly increasing diameter (Figure 3 (c), (d)) and pronounced surface corrugation. High-resolution TEM (Figure 3 (e)) shows lattice fringes with a separation of 0.775 nm along the wires, consistent with the spacing of (0002) basal planes in layered bulk GaS.[28] Selected-area electron diffraction (Figure 3 (c)) confirms that the nanowires are single-crystalline with symmetry axis aligned along the [0001] direction, *i.e.*, consist of stacks of GaS sheets arranged with their *c*-axis along the wire axis (Figure 3 (b)). A similar stacking has been observed previously for layered Ge(II) sulfide nanowires.[1,2] However, in contrast to nanowires of (orthorhombic) GeS, the sidewalls of type (ii) nanowires of (hexagonal)

GaS are not smooth. SEM and TEM images show stacks of few (average ~8, Figure 3 (h)) GaS sheets with about the same lateral size protruding substantially (up to ~50 nm) beyond the mean projected nanowire diameter (Figure 3 (f), (g)). Linear arrays of nanobeam electron diffraction patterns obtained along and across the nanowires (Figure S4, Figure S5) confirm high-quality monocrystalline GaS throughout. We note, however, that stacks of aligned or twinned sheets would give the same diffraction patterns, *i.e.*, would be indistinguishable in the diffraction analysis.

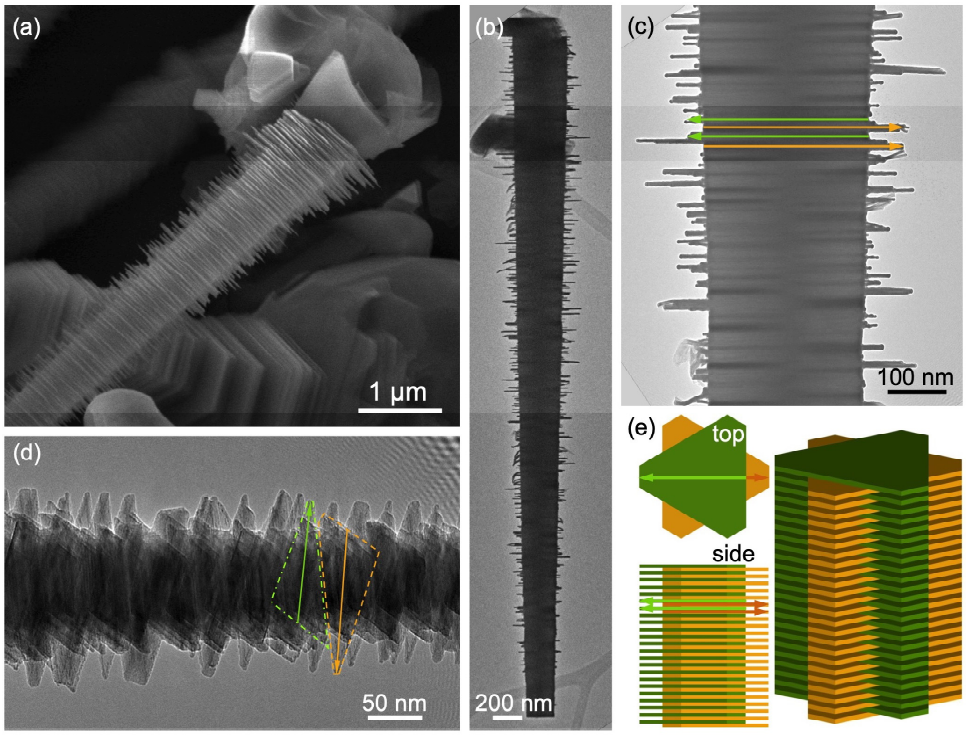

Figure 4. Twinning as the origin of the apparent surface roughness of type (ii) GaS van der Waals nanowires. (a) SEM image of a type (ii) GaS nanowire, showing the characteristic tapered shape and rough surface due to protruding stacks of GaS layers. **(b)** TEM image of a tapered type (ii) nanowire, oriented to show the relationship between flakes protruding on both sides of the wire. **(c)** Higher magnification view of a portion of the wire shown in (b). Arrows indicate flakes that protrude beyond the average thickness on the left (green) and right (yellow) edge of the wire. **(d)** Tilted TEM image showing the shape of the individual stacks of equally sized GaS flakes as triangles or truncated triangles. **(e)** Schematic illustrating the origin of the protruding layers seen in different projections in (b)-(c) and (d) as twinned (truncated) triangular few-layer stacks (top-, side-, and perspective views). A strong tendency toward forming such twinned stacks is also seen in SEM images of planar GaS flakes (*e.g.*, Fig. 1 (b)).

To understand the morphology of tapered type (ii) nanowires, in particular the observation that they consist of stacks of sheets with different apparent lateral sizes, we consider additional SEM as well as tilted TEM images shown in **Figure 4**. SEM (Figure 4 (a)) illustrates the general morphology of the protruding GaS sheets. Tilted TEM images, in which the wires are carefully rotated about their *c*-axis, show that in specific projections the protruding sheets alternate between opposite sides of the nanowires (Figure 4 (b), (c)). When combined with images with tilted *c*-axis (Figure 4 (d)), the following picture emerges. The tapered type (ii) nanowires generally consist of stacks of truncated triangular GaS flakes. Twins are introduced after ~8 GaS layers on average (Figure 3 (h)), so that the following truncated triangular stack is a mirror image of its predecessor (Figure 4 (e)). The side view of Figure 4 (e) illustrates that in certain projections, adjacent twins are seen as flakes protruding on alternating sides of the wire, as observed in Figure 4 (b), (c). Frequent twinning in the type (ii) nanowires is also supported by observations on the planar GaS nuclei covering our samples (Figure 1 (b)). Few-layer GaS flakes that make up the planar nuclei usually adopt triangular or truncated triangular shapes (typical growth shapes of few-layer GaS)[11,29] with frequent switching between two mirrored configurations (see Fig. S10). In contrast to other 2D materials such as GeS[1,30] and SnS,[31] which tend to form growth spirals centered around screw dislocations that enable growth without the need for nucleation, we find that layered GaS nanowires generally grow without dislocations. Adding a GaS sheet therefore requires nucleation on the preceding layer. While preserving the truncated triangular shape, the added nuclei show facile switching between twinned configurations to produce the characteristic pinecone-like surface roughness of the type (ii) GaS nanowires.

Despite their different morphologies, both type (i) and type (ii) nanowires grown with Ag catalysts carry large round particles at their tips (Figure 1 (a), (c)), which suggests that the nanowire growth generally proceeds *via* a VLS process, similar to other van der Waals nanowires.[1,2] In VLS growth, adsorption from the vapor phase increases the concentration of a solute in a liquid alloy catalyst, and the resulting supersaturation drives the incorporation of material (here GaS) at the liquid-solid interface to the nanowire. The catalyst drop in GaS nanowire growth likely involves a pseudo-binary alloy phase, analogous to the growth of other compound semiconductor nanowires (GeS, GaAs, InP, *etc.*).[32,33] Differences in the geometry of ribbon-like type (i) GaS nanowires and tapered type (ii) wires can be understood by considering the wetting of the quasi-binary (Ag-Ga) VLS drop, the vapor phase species incorporated into the catalyst, and the liquidus in the Ag-Ga phase diagram. The different orientation and facets in contact with the drop – exposed GaS edges for type (i) and basal planes for type (ii) nanowires – cause different contact angles between the drop and the nanowire tip, as seen in Figure 2 and Figure 3 (For a direct comparison, see Fig. S11). For the ribbon-like type (i) wires, the contact angle is very large, which results in the formation of thin wires largely independent of the volume of the catalyst. In contrast, for type (ii) nanowires the drop appears to wet the GaS basal plane with a reduced contact angle. Hence, the wire diameter will change with the drop volume. The tapered shape indicates a progressively increasing catalyst drop volume during growth. Indeed, a geometric analysis (Figure S6, Supporting Note 1) shows a 24-fold expansion of the volume of the drop, suggesting that part of the solute is retained in the catalyst.

In the evaporation of GaS, the precursor used here, the vapor consists predominantly of Ga_2S and S.[34] The expansion of the drop volume suggests that the two species are not equally incorporated into the catalyst, but Ga_2S is preferentially absorbed. The net growth of a GaS nanowire then

implies a reaction $Ga_2S \rightarrow GaS + Ga$ in the catalyst, where GaS adds to the growing nanowire and Ga accumulates in the catalyst drop. This scenario is consistent with the volume increase of the drop, and it explains the tapered nanowire shape. Since the Ag-Ga melting temperature decreases with increasing Ga content (Figure S6 (a)), the catalyst remains molten as its composition changes from initially ~30 at. % Ga to ~90 at. % Ga at the end of the growth. A comparison with Au catalyzed GaS nanowires (Figure S3), finally, shows key differences between Ag and Au catalysts. The smaller size of the Au-rich VLS catalysts suggests that the volume increase observed for Ag does not occur in the case of Au, *i.e.*, here the catalyst absorbs the vapor species Ga_2S and S at similar rates so that GaS nanowire growth leaves no excess Ga in the drop. Ag-based VLS catalysts are therefore especially suited for the growth of tapered GaS nanowires with progressively increasing diameter.

Raman spectroscopy of the GaS nanowires is summarized in **Figure 5**. Figure 5 (a) and Figure 5 (c) show optical images of larger (micrometer-scale) type (i) and type (ii) GaS nanowires, respectively, chosen to facilitate the diffraction-limited imaging and confocal Raman analysis. Corresponding micro-Raman maps of the A_{1g} mode intensity, shown in Figure 5 (b) and Figure 5 (d), confirm that the entire nanowires consist of layered GaS, in agreement hwith the TEM and diffraction results. The Raman spectrum in Figure 5 (e) shows the principal Raman active modes of GaS, identified as E_{1g} and E_{2g} modes arising from in-plane and A_{1g} modes corresponding to out-of-plane vibrations.[35,36] Figure 5 (f) is an optical image of a type (ii) nanowire, on which polarization-dependent Raman spectra were obtained. In these measurements (summarized in the polar plots of Figure 5 (g)) the angle φ between the polarization axis of the linearly polarized incident laser light and the nanowire axis was varied and Raman spectra recorded for each orientation. Both the E_{1g} mode and the A_{1g} mode show the two-fold symmetry expected in this

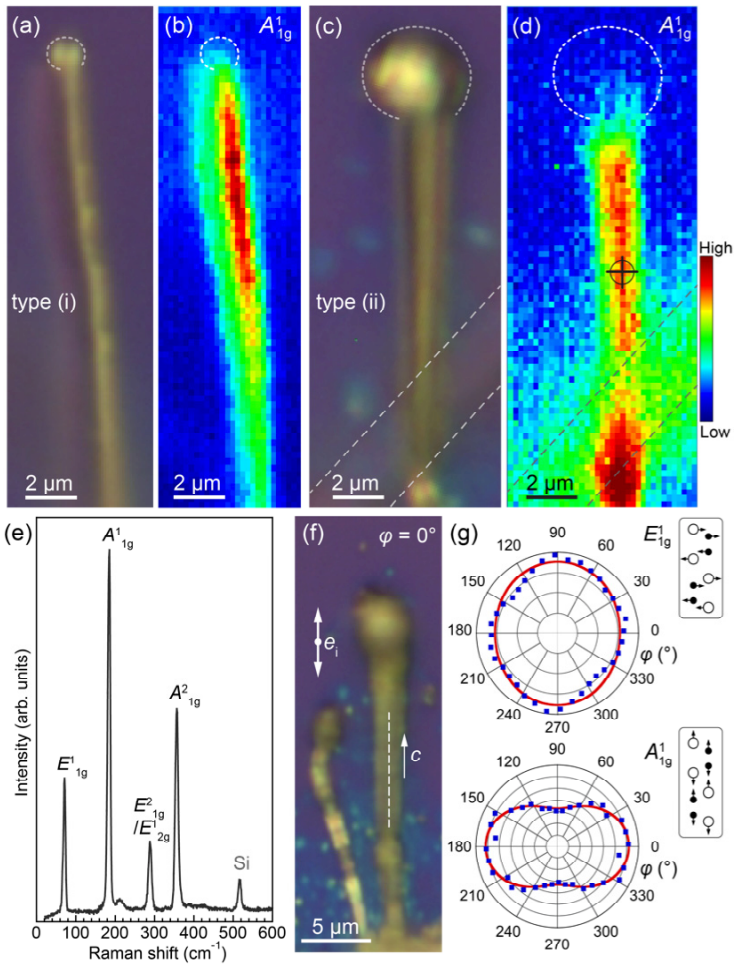

Figure 5. Micro-Raman spectroscopy of individual GaS nanowires. (a) Optical microscopy image of a ribbon-like type (i) GaS nanowire. **(b)** Raman map of the A^1_{1g} peak intensity (170-195 cm^{-1}) of the GaS nanowire shown in (a). **(c)** Optical microscopy image of a tapered type (ii) GaS nanowire. Dashed lines mark the position of a crossing wire outside the focal plane. **(d)** Raman map of the A^1_{1g} peak intensity (170-195 cm^{-1}) of the GaS nanowire shown in (c). Dotted lines in (a)-(c) mark the VLS catalysts at the tips of the nanowires. False color scale on the right applies to the Raman maps in (b) and (d). **(e)** Raman spectrum of the GaS nanowire, obtained in the area marked in (d). **(f)** Optical image of two type (ii) GaS nanowires. The wire on the right was used to measure polarization-dependent Raman spectra. e_i denotes the polarization axis of the linearly polarized incident laser light. **(g)** Polar plots of the E^1_{1g} and A^1_{1g} intensities as a function of the angle φ between the polarization axis and the *c*-axis of the GaS nanowire. Blue symbols: Experimental data. Red lines: Fits to the measured Raman intensities with angle dependences for the two modes as derived in Supporting Note 2. Insets on the right show the atomic displacements of the E^1_{1g} and A^1_{1g} normal modes (Filled symbols: Ga; open symbols: S).

scattering geometry (see Supporting Note 2, Fig. S9), consistent with a single crystalline structure of type (ii) nanowires with van der Waals layering (GaS *c*-axis) along the nanowire axis.

Optoelectronics of Individual GaS van der Waals Nanowires

To investigate the optoelectronic properties of the monocrystalline GaS van der Waals nanowires, we probed their optical absorption using valence electron energy loss spectroscopy (EELS) with energy resolution of ~65 meV in monchromated STEM, and light emission by cathodoluminescence spectroscopy in STEM (STEM-CL). Both types of measurements were carried out with electron probe sizes below 1 nm, enabling absorption measurements, the mapping of light emission, and acquisition of luminescence spectra and hyperspectral scans for individual nanowires.

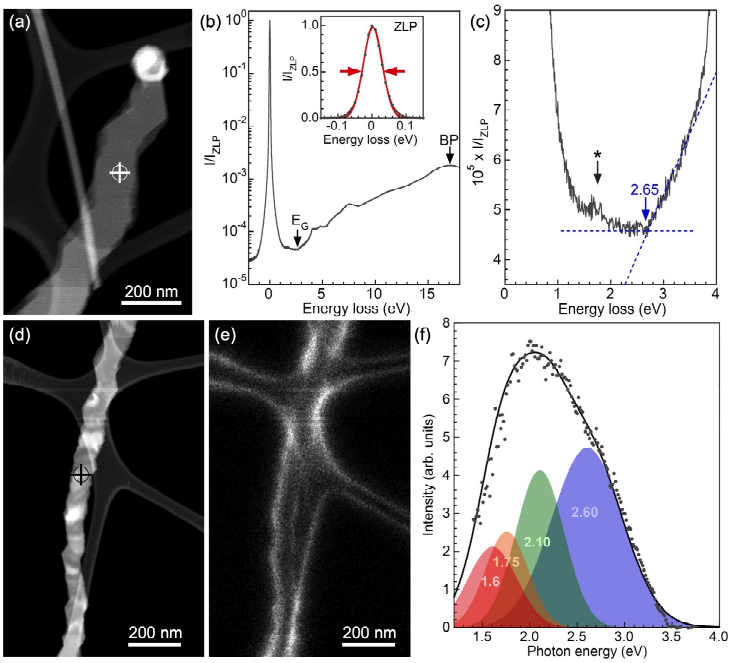

Figure 6. Optoelectronics of individual ribbon-like type (i) GaS nanowires with *c*-axis perpendicular to the nanowire axis. (a) HAADF-STEM image of a section of an as-grown ribbon-like GaS nanowire. **(b)** Monochromated STEM-EELS spectrum obtained at the position indicated in (a). E_G: Fundamental band gap; BP: Bulk plasmon. Inset: Gaussian fit to the zero-loss peak (ZLP), showing a full-width at half maximum of 65 meV. **(c)** Magnified view of the band gap region of the spectrum, showing a sharp onset at the fundamental band gap (2.65 eV) along with features in the gap region (*) whose energy coincides with luminescence peaks (panel (f)). **(d)** HAADF-STEM image of a ribbon-like GaS nanowire. **(e)** Panchromatic CL map of the nanowire shown in (d). **(f)** CL spectrum obtained at the position indicated in (d). Shaded regions represent a series of Gaussian fits to the spectrum, with central photon energies as indicated (in eV).

Typical results for ribbon-like type (i) nanowires are summarized in **Figure 6**. Single nanowire absorption measurements by EELS (Figure 6 (a)-(c)) show a characteristic energy loss onset – associated with interband transitions across the fundamental bandgap – at E_g = 2.65 eV, close to the previously reported bandgap of GaS.[37,38] Features between 3-10 eV are likely associated with special points in the GaS dielectric function seen previously,[39,40] while the peak at ~17 eV has been explained by an excitation of the GaS bulk plasmon.[8,41] At low energy (in the gap region), the spectra show structure with intensity above the noise level whose energy coincides with emission features observed in CL (see below), *i.e.*, which may be associated with losses due to transitions between gap states. STEM-CL (Figure 6 (d)-(f)) shows the brightest luminescence from the edges of the ribbon-like GaS nanowires. CL spectra show a strong interband emission (photon energy hν ~ 2.6 eV) and additional luminescence from transitions in the gap whose energies (hν ~ 2.1 eV, 1.75 eV, and 1.6 eV) are consistent with donor-acceptor recombination between defect (S and Ga vacancy) levels within the bandgap of bulk GaS,[42-44] as well as recombination from the conduction band edge to hole centers near the valence band edge.[45]

While the optoelectronics of ribbon-like type (i) nanowires are similar to those of GaS flakes,[11] the tapered type (ii) GaS nanowires show interesting additional photonic properties due to their particular morphology, *i.e.*, the van der Waals stacking of few-layer flakes with *c*-axis parallel to the wire axis. **Figure 7** summarizes STEM-CL results for a single tapered GaS wire with thickness ranging from 170 nm (root) to 360 nm (tip). STEM reflects the characteristic surface morphology with protruding flakes, as discussed above (Figure 7 (a)). Panchromatic STEM-CL maps again show intense visible-light emission from the near-surface region, similar to type (i) wires, but also a modulated emission intensity within the nanowire whose pattern is dependent on the wire thickness (Figure 7 (b)). Sets of CL spectra were collected in two hyperspectral linescans, along and across the nanowire as indicated in Figure 7 (a). The linescan along the

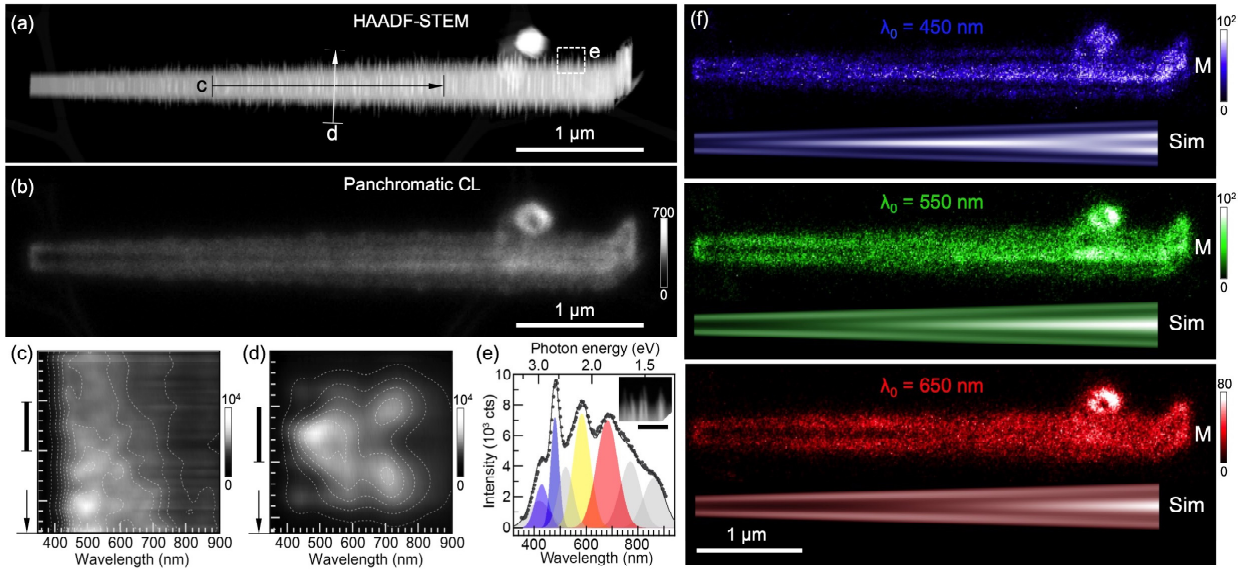

Figure 7. STEM-CL on individual type (ii) GaS nanowires (T = 103 K). (a) STEM image of a section of an as-grown GaS nanowire. **(b)** Panchromatic CL map of the GaS nanowire shown in (a). **(c)** Hyperspectral linescan across the nanowire, following line "c" marked in (a). Arrow: Linescan direction, as shown in (a). Vertical scale bar: 500 nm real-space distance. **(d)** Hyperspectral line scan along the nanowire, following line "d" marked in (a). Arrow: Linescan direction, as shown in (a). Vertical scale bar: 100 nm real-space distance. **(e)** Local luminescence spectrum from one of the protruding GaS flakes near the tip of the nanowire (inset, scale bar: 100 nm), marked by rectangle "e" in (a). Shaded areas represent Gaussian fits to the experimental spectrum. **(f)** Monochromatic CL maps (bandwidth 50 nm) of the GaS nanowire shown in (a) for (free-space) center wavelengths λ_0 = 450 nm, 550 nm, and 650 nm. "M": Measured intensity maps. "Sim": Simulated intensity distribution as discussed in the text and in Supporting Note 2. False color scales in panels (b), (c), (d), and (f) represent measured intensities (total counts).

central nanowire axis (Figure 7 (c)) shows emission maxima for $\lambda \sim 480$ nm and $\lambda \sim 580$ nm (*i.e.*, photon energy hν ~2.58 eV and 2.14 eV). Significant emission extends in a tail to longer wavelengths. Comparing with reported absorption measurements that give an indirect bandgap of GaS of 2.53 eV (T = 300 K)[37,38] and 2.5-2.6 eV (T = 77 K),[46] as well as our EELS results showing E_g = 2.65 eV for (few nm) thin single type (i) nanowires (Figure 6), we can assign the strong CL emission at ~ 2.58 eV to band-edge luminescence. The linescan of Figure 7 (c) shows other notable features. Firstly, the luminescence intensity increases with increasing thickness along the wire, consistent with the well-known thickness dependent rate of electronic excitation

by the electron beam in CL.[47] And secondly, the spectral features – both the short-wavelength emission onset and especially the long-wavelength tail (see contour lines in Fig. 7 (c)) – show a clear red shift with increasing thickness of the tapered nanowire, indicating that lateral carrier confinement within the finite-size van der Waals sheets (in contrast to the vertical confinement seen previously in few-layer GeS)[8,10] begins to play a role below a thickness of ~300 nm. Hyperspectral linescans across the nanowires show similar spectral features near the center, but a redistribution of the emitted intensity near the surface (Figure 7 (d)). The near-surface luminescence is examined further in the CL spectrum of Figure 7 (e). The peak with highest emission intensity (λ = 480.0 ± 18.6 nm; hν ~2.58 eV) originates from the interband transition across the indirect gap of GaS. A higher energy peak (λ = 429.0 ± 30 nm; 2.89 eV) is likely due to recombination across the direct bandgap, whereas peaks at longer wavelengths (λ = 583.6 ± 38.3 nm; 2.12 eV. λ = 681.5 ± 48.4 nm; 1.82 eV) are due to defect states in the gap.

Photoluminescence (PL) measurements of bulk and few layer GaS flakes frequently show broad asymmetric emission bands covering the visible range.[11,48,49] Room-temperature PL of ensembles of GaS nanostructures such as nanohorns,[25] and nanobelts[26] shows a broad peak centered at 580 nm and extending between 400-800 nm. PL of GaS nanotubes shows two strong emission bands centered at 585 nm (2.12 eV) and 615 nm (2.02 eV).[23] The ubiquitous long wavelength (sub-bandgap) PL emission is mainly attributed to the presence of structural defects such as S vacancies (creating a donor level) and Ga vacancies (acceptor), which leads to emission due to radiative recombination of donor-acceptor pairs.[43,44] The emission at 583.6 nm (2.12 eV) as well as the observed intensity towards longer wavelengths must have a similar defect origin. The emission near 700 nm is strongly enhanced near the surface (Figure 7 (d)), indicating a higher abundance of gap states in the near-surface region.

Finally, both the panchromatic CL map (Figure 7 (b)) and the transverse spectrum linescan (Figure 7 (d)) show a pronounced thickness dependent modulation of the luminescence intensity across the tapered GaS nanowires. To uncover its origin, we acquired monochromatic CL intensity maps at several wavelengths. Figure 7 (f) shows three examples, with (vacuum) center wavelengths λ_0 = 450 nm, 550 nm, and 650 nm (pass band: ± 25 nm). The characteristic intensity patterns can be reproduced by considering interference of traveling waveguide photonic modes in the GaS nanowires. In STEM-CL, photon emission excited by the localized electron beam launches photonic modes, whose specular reflection by surface facets coherently superimposes them with the primary photons to produce an interference pattern.[50] In tapered type (ii) GaS nanowires, most points (except near the ends) are too far from reflective facets to produce longitudinal waveguide mode interference, but reflection from the side facets can give rise to transverse interference patterns (Figure S7). Further analysis (see Supporting Note 2) shows the photonic waveguide modes to be insensitive to the twinning-induced surface corrugation; instead, the confined modes appear to be efficiently reflected by the hexagonal nanowire core. This is confirmed by comparing the measured CL maps with simulated interference fringe patterns using the actual geometry of the nanowire shown in Figure 7, the reported dispersion of the GaS refractive index n (which defines the wavelength $\lambda^{wg} = \lambda_0 n^{-1}$ of the waveguide mode),[50,51] and specular reflection by a hexagonal envelope of side facets; the simulated waveguide mode interference patterns closely match the measured monochromatic STEM-CL maps of individual nanowires for a particular orientation of the wire relative to the exciting electron beam (Figure S7 (c), (d)).

Conclusions

We have discussed nanowires from the layered van der Waals material GaS. Vapor-liquid-solid growth over Ag catalysts produces two types of single-crystalline nanowires: Ribbon-like (type (i)) wires with van der Waals stacking perpendicular to the nanowire axis, uniform width and typical length exceeding 10 μm; and (type (ii)) wires with layers stacked along their axis, tapered shape with increasing thickness from root to tip, and several μm length. The two morphologies result from different wetting properties of the Ag-rich catalyst on the open edges (type (i)) and basal plane (type (ii)) of GaS. In contrast, VLS growth with Au catalysts produces only ribbon-like nanowires. Both types of nanowires, readily grown as high-quality single-crystals, show properties interesting for optoelectronic applications, notably a bandgap of 2.65 eV and intense band-edge emission in the blue region of the visible spectrum. In addition, the wires emit at several energies within the bandgap due to defect states characteristic of GaS. In contrast to planar monolayer or few-layer flakes, the layered GaS nanowires – in particular the type (ii) morphology with layers stacked along the wire axis and subject to quasi-periodic twinning – expose a high density of open layer edges, *i.e.*, a large number of dangling bonds. Whereas measurements on individual nanowires suggest that the abundant edges do not negatively affect optoelectronic and photonic properties, such as efficient light emission and interference of confined waveguide photonic modes, the open edges of the triangular sheets making up the wires promise additional functionality, such as enhanced chemical reactivity associated with the edges of layered crystals[7] for photo- or electrocatalysis and facile access to the van der Waals interlayer space for intercalation-type energy storage applications.

Methods

GaS Nanowire Growth. GaS nanowires were synthesized using a GaS powder precursor (99.99%, ProChem, Inc.) in a quartz tube reactor consisting heated by a furnace with two

independently controlled temperature zones. The evaporation zone containing a quartz boat with the GaS powder was heated to 850°C. The zone containing the substrate was heated to growth temperatures T_s of 450-650°C. 300 nm thick SiO_2/Si wafers covered with nominally 2-4 nm thick Ag or Au films deposited by magnetron sputtering at room temperature were used as substrates. The thin Au or Ag films dewet at the growth temperature to form polydisperse nanoparticle ensembles.[27,52] During growth a H_2 (2%)/Ar carrier gas flow was maintained at 60 standard cubic centimeters per minute (sccm) and a pressure of 20 mTorr. The growth was typically performed for 20 minutes. Growth on Au films resulted in the formation of GaS films, flakes and ribbon-like nanowires, while the growth on Ag catalysts produced groups of the two types of GaS nanowires discussed in the text, surrounded by planar flakes. Upon completion of each growth, the system naturally cooled to room temperature.

Electron Microscopy and Diffraction. The morphology of the GaS flakes, ribbons and nanowires was investigated by SEM in a FEI Helios Nanolab 660 field-emission microscope at 5 keV primary beam energy, and by TEM, HAADF-STEM, and nanobeam electron diffraction in an FEI Talos F200X field-emission microscope operated at 200 kV. For the TEM investigations, the nanowires/flakes were dry-transferred onto amorphous C films supported by Cu grids.

Raman Spectroscopy. Characterization of the as-grown GaS nanowires on the SiO_2/Si substrates was carried out by micro-Raman spectroscopy, Raman mapping, and polarization-dependent Raman spectroscopy using a confocal Raman microscope (Horiba Xplora plus) with lateral resolution of ~0.5 μm. The measurements used an excitation wavelength of 532 nm, 100x objective, laser power of 16.8 μW, and a 1800 lines/mm grating. Polarized Raman spectroscopy used a linear-polarized incident laser beam, whose polarization axis was systematically rotated

relative to the *c*-axis of the GaS nanowires. No analyzer was used for the scattered light, hence the measured signal corresponds closely to the parallel polarization geometry.

Single Nanowire Optoelectronics. The optoelectronic properties of individual GaS nanowires were investigated by both local absorption and luminescence spectroscopy. Absorption was measured by valence electron energy-loss spectroscopy in monochromated STEM in a Nion Hermes aberration-corrected electron microscope (at Oak Ridge National laboratory) operated at 60 kV. Light emission from individual GaS nanowires was probed by cathodoluminescence (CL) measurements performed in STEM mode (STEM-CL) using a Gatan Vulcan CL holder at room temperature and 100 K and 200 kV electron energy. The current of the exciting electron beam was typically 300-600 pA. Panchromatic CL maps (Figure 6 (e), Figure 7 (e)) were acquired with 512×512 pixels and integration time of 1.28 ms per pixel. Monochromatic CL maps (Figure 7 (f)) were obtained with a bandpass of ±25 nm around the chosen center wavelength, 512×512 pixels and integration time of 1.28 ms per pixel. Hyperspectral line scans were acquired by rastering the electron beam in small steps across individual nanowires and acquiring full CL spectra at each beam position (integration time: 10 seconds per spectrum). Local STEM-CL spectra were acquired by positioning the focused electron beam excitation at chosen locations and integrating the spectrometer output detected by a Si CCD array detector for 10-20 seconds.

Acknowledgements

This work was supported by the National Science Foundation, Division of Materials Research, Solid State and Materials Chemistry Program under Grant No. DMR-1904843 and sponsored by the Department of the Navy, Office of Naval Research under ONR award number N00014-20-1-2305. The monochromated EELS was supported by the Center for Nanophase Materials Sciences, which is a DOE Office of Science User Facility, using instrumentation within ORNL's

Materials Characterization Core provided by UT-Batelle, LLC under Contract No. DE-AC05-00OR22725 with the U.S. Department of Energy and sponsored by the Laboratory Directed Research and Development Program of Oak Ridge National Laboratory, managed by UT-Battelle, LLC, for the U.S. Department of Energy.

Supporting Information Available: Supplementary Figures S1-S8: TEM of ultrathin ribbon-like GaS nanowires; Characterization of GaS flakes and ribbon-like GaS nanowires synthesized over Au catalysts; Nanobeam diffraction on tapered GaS nanowires; Estimated volume change of the Ag-rich catalyst during GaS nanowire growth; STEM-CL of a hexagonal GaS nanowire; Interference of confined photonic waveguide modes in tapered GaS nanowires; Predicted polarized Raman intensity distribution; Twinning in planar GaS flakes; Contact angles between type (i) and type (ii) GaS nanowires and Ag-rich VLS catalysts.

Supporting Notes: Volume and composition evolution of the Ag VLS catalyst; Polarized Raman spectroscopy; Confined photonic waveguide modes in GaS nanowires.

This material is available free of charge *via* the Internet at http://pubs.acs.org.

References

1. Sutter, P.; Wimer, S.; Sutter, E. Chiral Twisted van der Waals Nanowires. *Nature* **2019**, *570*, 354-357.
2. Sutter, E.; Sutter, P. 1D Wires of 2D Layered Materials: Germanium Sulfide Nanowires as Efficient Light Emitters. *ACS Appl. Nano Mater.* **2018**, *1*, 1042-1049.
3. Li, C.; Yu, Y. F.; Chi, M. F.; Cao, L. Y. Epitaxial Nanosheet-Nanowire Heterostructures. *Nano Lett.* **2013**, *13*, 948-953.
4. Deepak, F. L.; Esparza, R.; Borges, B.; López-Lozano, X.; Jose-Yacaman, M. Rippled and Helical MoS2 Nanowire Catalysts: An Aberration Corrected STEM Study. *Catal. Lett.* **2011**, *141*, 518-524.
5. Peng, H.; Meister, S.; Chan, C. K.; Zhang, X. F.; Cui, Y. Morphology Control of Layer-Structured Gallium Selenide Nanowires. *Nano Lett.* **2007**, *7*, 199-203.

6. Chhowalla, M.; Shin, H. S.; Eda, G.; Li, L.-J.; Loh, K. P.; Zhang, H. The Chemistry of Two-Dimensional Layered Transition Metal Dichalcogenide Nanosheets. *Nat. Chem.* **2013**, *5*, 263-275.
7. Harvey, A.; Backes, C.; Gholamvand, Z.; Hanlon, D.; McAteer, D.; Nerl, H. C.; McGuire, E.; Seral-Ascaso, A.; Ramasse, Q. M.; McEvoy, N.; Winters, S.; Berner, N. C.; McCloskey, D.; Donegan, J. F.; Duesberg, G. S.; Nicolosi, V.; Coleman, J. N. Preparation of Gallium Sulfide Nanosheets by Liquid Exfoliation and Their Application as Hydrogen Evolution Catalysts. *Chem. Mater.* **2015**, *27*, 3483-3493.
8. Hu, P.; Wang, L.; Yoon, M.; Zhang, J.; Feng, W.; Wang, X.; Wen, Z.; Idrobo, J. C.; Miyamoto, Y.; Geohegan, D. B.; Xiao, K. Highly Responsive Ultrathin GaS Nanosheet Photodetectors on Rigid and Flexible Substrates. *Nano Lett.* **2013**, *13*, 1649-1654.
9. Chen, T.; Lu, Y.; Sheng, Y.; Shu, Y.; Li, X.; Chang, R.-J.; Bhaskaran, H.; Warner, J. H. Ultrathin All-2D Lateral Graphene/GaS/Graphene UV Photodetectors by Direct CVD Growth. *ACS Appl. Mater. Interf.* **2019**, *11*, 48172-48178.
10. Yang, S.; Li, Y.; Wang, X.; Huo, N.; Xia, J.-B.; Li, S.-S.; Li, J. High Performance Few-Layer GaS Photodetector and Its Unique Photo-Response in Different Gas Environments. *Nanoscale* **2014**, *6*, 2582-2587.
11. Jung, C. S.; Shojaei, F.; Park, K.; Oh, J. Y.; Im, H. S.; Jang, D. M.; Park, J.; Kang, H. S. Red-to-Ultraviolet Emission Tuning of Two-Dimensional Gallium Sulfide/Selenide. *ACS Nano* **2015**, *9*, 9585-9593.
12. Chitara, B.; Ya'akobovitz, A. Elastic Properties and Breaking Strengths of GaS, GaSe and GaTe Nanosheets. *Nanoscale* **2018**, *10*, 13022-13027.
13. Pham, K. D.; Vi, V. T. T.; Thuan, D. V.; Hieu, N. V.; Nguyen, C. V.; Phuc, H. V.; Hoi, B. D.; Phuong, L. T. T.; Cuong, N. Q.; Lu, D. V.; Hieu, N. N. Tuning the Electronic Properties of GaS Monolayer by Strain Engineering and Electric Field. *Chem. Phys.* **2019**, *524*, 101-105.
14. Zhu, Z.; Cheng, Y.; Schwingenschlögl, U. Topological Phase Transition in Layered GaS and GaSe. *Phys. Rev. Lett.* **2012**, *108*, 266805.
15. Zhang, Y.; Yang, Z. Efficient Band Structure Engineering and Visible-Light Response in ZrS2/GaS Heterobilayer by Electrical Field or External Strains. *Phys. Lett. A* **2019**, *383*, 2969-2973.
16. Li, X.-H.; Wang, B.-J.; Cai, X.-L.; Zhang, L.-W.; Wang, G.-D.; Ke, S.-H. Tunable Electronic Properties of Arsenene/GaS van der Waals Heterostructures. *RSC Adv.* **2017**, *7*, 28393-28398.
17. Keldysh, L. V. The Electron-Hole Liquid in Semiconductors. *Contemp. Phys.* **1986**, *27*, 395-428.
18. Belen'kij, G.; Godzhaev, M.; Salaev, E.; Aliev, E. High Temperature Electron-Hole Liquid in Layered Crystals InSe, GaSe, GaS. *Sov. Phys. JETP* **1986**, *64*, 1117-1123.
19. Strojnik, M.; Kovic, A.; Mrzel, A.; Buh, J.; Strle, J.; Mihailovic, D. MoS2 Nanotube Field Effect Transistors. *AIP Adv.* **2014**, *4*, 097114.
20. Seifert, G.; Terrones, H.; Terrones, M.; Jungnickel, G.; Frauenheim, T. Structure and Electronic Properties of MoS2 Nanotubes. *Phys. Rev. Lett.* **2000**, *85*, 146-149.

21. Radovsky, G.; Popovitz-Biro, R.; Tenne, R. Study of Tubular Structures of the Misfit Layered Compound SnS2/SnS. *Chem. Mater.* **2012**, *24*, 3004-3015.
22. Zhang, C.; Ning, Z.; Liu, Y.; Xu, T.; Guo, Y.; Zak, A.; Zhang, Z.; Wang, S.; Tenne, R.; Chen, Q. Electrical Transport Properties of Individual WS2 Nanotubes and Their Dependence on Water and Oxygen Absorption. *Appl. Phys. Lett.* **2012**, *101*, 113112.
23. Hu, J. Q.; Bando, Y.; Zhan, J. H.; Liu, Z. W.; Golberg, D. Uniform and High-Quality Submicrometer Tubes of GaS Layered Crystals. *Appl. Phys. Lett.* **2005**, *87*, 153112.
24. Enyashin, A. N.; Brontvein, O.; Seifert, G.; Tenne, R. Structure and Stability of GaS Fullerenes and Nanotubes. *Isr. J. Chem.* **2017**, *57*, 529-539.
25. Sinha, G.; Panda, S. K.; Datta, A.; Chavan, P. G.; Shinde, D. R.; More, M. A.; Joag, D. S.; Patra, A. Controlled Growth of Well-Aligned GaS Nanohornlike Structures and Their Field Emission Properties. *ACS Appl. Mater. Interf.* **2011**, *3*, 2130-2135.
26. Shen, G.; Chen, D.; Chen, P.-C.; Zhou, C. Vapor−Solid Growth of One-Dimensional Layer-Structured Gallium Sulfide Nanostructures. *ACS Nano* **2009**, *3*, 1115-1120.
27. Sutter, E.; Sutter, P. Axial Heterostructures with Phase-Controlled Metastable Segments via Post-Growth Reactions of Ge Nanowires. *Chem. Mater.* **2019**, *31*, 8174-8181.
28. Pardo, M. P.; Guittard, M.; Chilouet, A.; Tomas, A. Diagramme de Phases Gallium-Soufre et Etudes Structurales des Phases Solides. *J. Solid State Chem.* **1993**, *102*, 423-433.
29. Wang, X.; Sheng, Y.; Chang, R.-J.; Lee, J. K.; Zhou, Y.; Li, S.; Chen, T.; Huang, H.; Porter, B. F.; Bhaskaran, H.; Warner, J. H. Chemical Vapor Deposition Growth of Two-Dimensional Monolayer Gallium Sulfide Crystals Using Hydrogen Reduction of Ga2S3. *ACS Omega* **2018**, *3*, 7897-7903.
30. Sutter, E.; Zhang, B.; Sun, M.; Sutter, P. Few-Layer to Multilayer Germanium(II) Sulfide: Synthesis, Structure, Stability, and Optoelectronics. *ACS Nano* **2019**, *13*, 9352-9362.
31. Sutter, P.; Sutter, E. Growth Mechanisms of Anisotropic Layered Group IV Chalcogenides on van der Waals Substrates for Energy Conversion Applications. *ACS Appl. Nano Mater.* **2018**, *1*, 3026-3034.
32. Panish, M. B. Ternary Condensed Phase Systems of Gallium and Arsenic with Group Ib Elements. *J. Electrochem. Soc.* **1967**, *114*, 516-&.
33. Duan, X.; Lieber, C. M. General Synthesis of Compound Semiconductor Nanowires. *Adv. Mater.* **2000**, *12*, 298-302.
34. Mills, K. C., *Thermodynamic Data for Inorganic Sulphides, Selenides and Tellurides*. Butterworths: London, 1974; p 310-314.
35. van der Ziel, J. P.; Meixner, A. E.; Kasper, H. M. Raman Scattering from β-GaS. *Solid State Commun.* **1973**, *12*, 1213-1215.
36. Alencar, R. S.; Rabelo, C.; Miranda, H. L. S.; Vasconcelos, T. L.; Oliveira, B. S.; Ribeiro, A.; Públio, B. C.; Ribeiro-Soares, J.; Filho, A. G. S.; Cançado, L. G.; Jorio, A. Probing Spatial Phonon Correlation Length in Post-Transition Metal Monochalcogenide GaS Using Tip-Enhanced Raman Spectroscopy. *Nano Lett.* **2019**, *19*, 7357-7364.
37. Ho, C. H.; Lin, S. L. Optical Properties of the Interband Transitions of Layered Gallium Sulfide. *J. Appl. Phys.* **2006**, *100*, 083508.
38. Shigetomi, S.; Sakai, K.; Ikari, T. Photoluminescence of Layered Semiconductor GaS Doped with Mn. *Phys. Status Solidi B* **2004**, *241*, 2607-2612.

39. Giorgianni, U.; Mondio, G.; Perillo, P.; Saitta, G.; Vermiglio, G. Infrared and UV-Visible Spectra of Layer Semiconductors GaS, GaSe and GaTe. *J. Phys.* **1977**, *38*, 1293-1299.
40. Piacentini, M.; Olson, C. G.; Balzarotti, A.; Girlanda, R.; Grasso, V.; Doni, E. Electronic Properties of the III-VI Layer Compounds GaS, GaSe, and InSe. III. Reflectivity from 4 to 32 eV. *Nuovo Cimento B* **1979**, *54*, 248-268.
41. Soukiassian, P.; Cazaux, J.; Perrin, J. Electronic Excitations (3 to 35 eV Range) in Some Layered III–VI Compounds: GaS, GaSe, and InSe. *Phys. Status Solidi B* **1974**, *66*, 151-160.
42. Aydinli, A.; Gasanly, N. M.; Gökşen, K. Donor–Acceptor Pair Recombination in Gallium Sulfide. *J. Appl. Phys.* **2000**, *88*, 7144-7149.
43. Shigetomi, S.; Ikari, T. Optical Properties of Layered Semiconductor GaS Doped with As. *J. Appl. Phys.* **2007**, *102*, 033701.
44. Belenkii, G. L.; Godzhaev, M. O. Excitons in Gallium Sulphide. *Phys. Status Solidi B* **1978**, *85*, 453-458.
45. de Blasi, C.; Galassini, S.; Micocci, G.; Tepore, A.; Manfredotti, C. Hole Centres in n-GaS. *Phys. Status Solidi A* **1980**, *58*, 609-613.
46. Aulich, E.; Brebner, J. L.; Mooser, E. Indirect Energy Gap in GaSe and GaS. *Phys. Status Solidi B* **1969**, *31*, 129-131.
47. García de Abajo, F. J. Optical Excitations in Electron Microscopy. *Rev. Mod. Phys.* **2010**, *82*, 209-275.
48. Shevitski, B.; Ulstrup, S.; Koch, R. J.; Cai, H.; Tongay, S.; Moreschini, L.; Jozwiak, C.; Bostwick, A.; Zettl, A.; Rotenberg, E.; Aloni, S. Tunable Electronic Structure in Gallium Chalcogenide van der Waals Compounds. *Phys. Rev. B* **2019**, *100*, 165112.
49. Catalano, I. M.; Ferrara, M.; Tantalo, P. Luminescence and Photocurrent of Gallium Sulphide. *Phys. Status Solidi A* **1973**, *20*, K135-K138.
50. Sutter, P.; Argyropoulos, C.; Sutter, E. Germanium Sulfide Nano-Optics Probed by STEM-Cathodoluminescence Spectroscopy. *Nano Lett.* **2018**, *18*, 4576-4583.
51. McMath, T. A.; Irwin, J. C. Indices of Refraction of GaS and GaSe. *Phys. Status Solidi A* **1976**, *38*, 731-738.
52. Sutter, E.; Ozturk, B.; Sutter, P. Selective Growth of Ge Nanowires by Low-Temperature Thermal Evaporation. *Nanotechnology* **2008**, *19*, 435607.

TOC Graphic

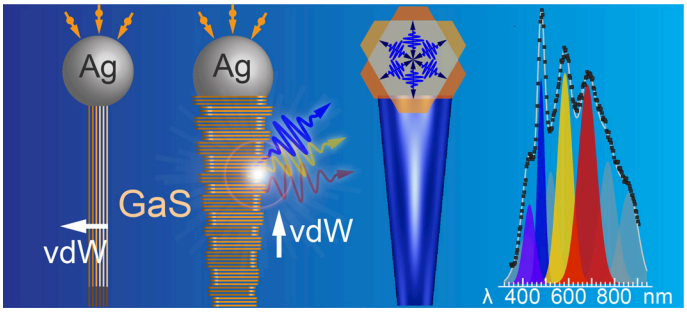

Supporting Information

Vapor-Liquid-Solid Growth and Optoelectronics of Gallium Sulfide van der Waals Nanowires

Eli Sutter,[1,*] Jacob S. French,[2] Stephan Sutter,[2] Juan Carlos Idrobo,[3] and Peter Sutter[2,*]

[1]Department of Mechanical & Materials Engineering, University of Nebraska-Lincoln, Lincoln, Nebraska 68588, USA
E-mail: esutter@unl.edu

[2]Department of Electrical & Computer Engineering, University of Nebraska-Lincoln, Lincoln, Nebraska 68588, USA
E-mail: psutter@unl.edu

[3]Center for Nanophase Materials Sciences, Oak Ridge National Laboratory, Oak Ridge, TN 37831, United States

Supporting Figures

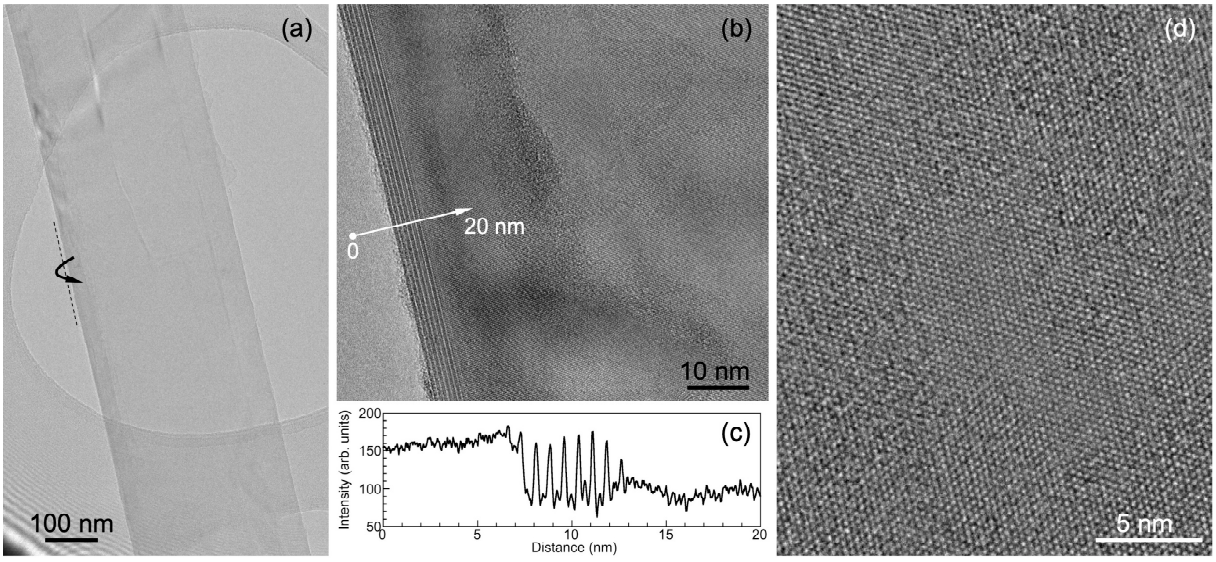

Figure S1. Ultrathin ribbon-like type (i) GaS nanowires. (a) TEM image of a type (i) GaS nanowire with folded edge, as indicated (arrow). **(b)** High-resolution TEM image near the edge, showing the GaS layering along the folded region. **(c)** Intensity line profile along the arrow marked in (b) showing 8 intensity maxima, *i.e.*, a thickness of 8 GaS monolayers. **(d)** High-resolution TEM image obtained within the nanowire, showing the hexagonal structure of basal-plane oriented GaS (zone axis, ZA: [0001]).

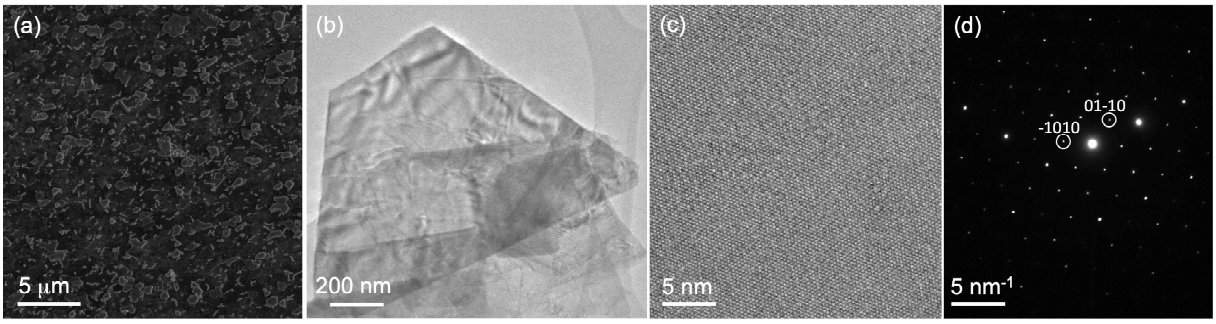

Figure S2. GaS flakes grown on Au catalyst on SiO_2. (a) SEM image of a section of an as-grown GaS on SiO_2/Si covered with a thin Au film. **(b)** Typical GaS flakes dry transferred to a carbon TEM grid. **(c)** High-resolution TEM image, showing the characteristic hexagonal structure of basal-plane oriented GaS. **(d)** Selected-area electron diffraction pattern (zone axis, ZA: [0001]) of the flake.

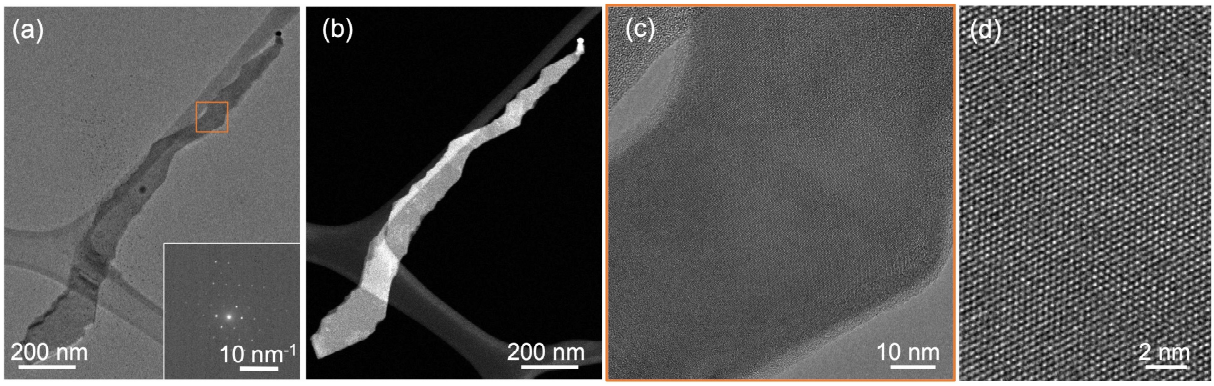

Figure S3. Ribbon-like type (i) GaS nanowires grown with Au catalysts on SiO_2. (a) TEM image of a ribbon-like GaS nanowire synthesized by VLS growth with Au catalyst. Note the small Au-rich particle at the tip (upper right). Inset: Selected-area electron diffraction pattern (Zone axis, ZA: 0001). **(b)** HAADF-STEM image of the GaS nanowire shown in (a). **(c)** Magnified view of the area marked by a rectangle in (a). **(d)** High-resolution TEM image of the basal-plane GaS lattice structure.

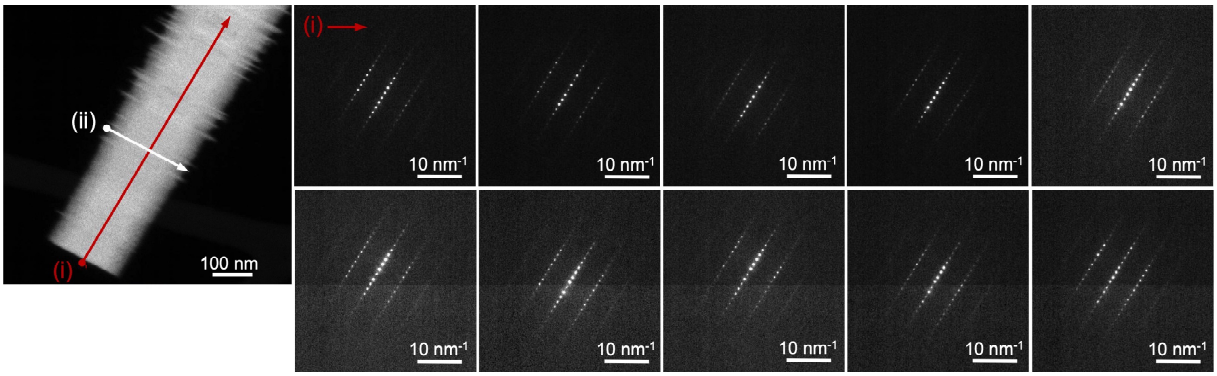

Figure S4. Nanobeam diffraction along a tapered type (ii) GaS nanowire. (a) HAADF-STEM image obtained near the thinner end of the nanowire. **(b)** Nanobeam diffraction patterns obtained along the nanowire (line marked (i) in panel (a)). The series comprises every 5th diffraction pattern of a total of 50 patterns acquired along the line (i) shown in (a).

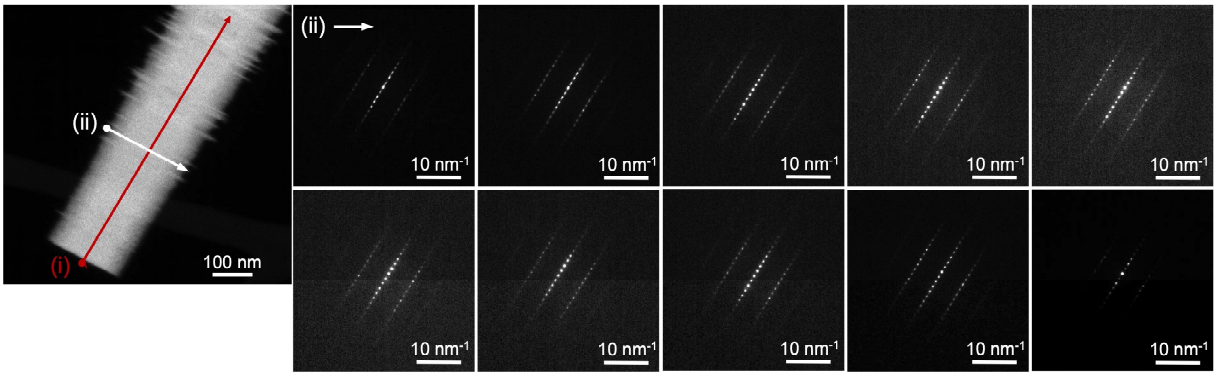

Figure S5. Nanobeam diffraction across a tapered type (ii) GaS nanowire. (a) HAADF-STEM image obtained near the thinner end of the nanowire. **(b)** Nanobeam diffraction patterns obtained across the nanowire (line marked (ii) in panel (a)). The series comprises every 3rd diffraction pattern of a total of 30 patterns acquired along the line (ii) shown in (a).

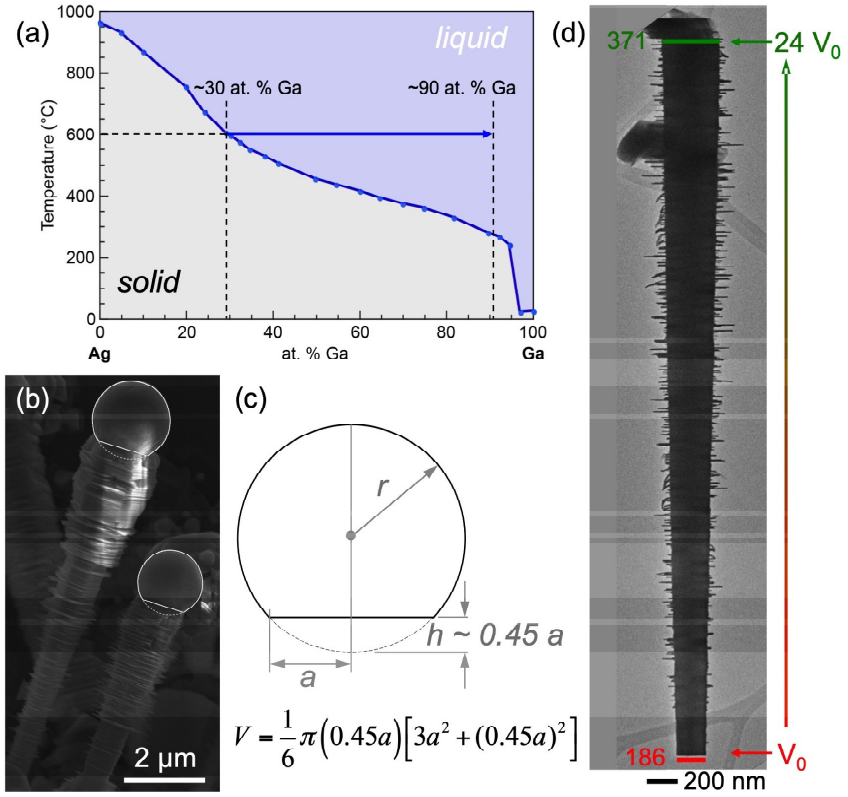

Figure S6. Estimation of the size evolution of the VLS catalyst during growth of tapered type (ii) GaS nanowires. (a) Partial Ag-Ga phase diagram, showing the composition-dependent liquidus line of the binary alloy. Note: Growth temperature in our experiments is 600°C. Arrow: Evolution of the Ga content from an initial catalyst with composition that corresponds to a melting temperature of 600°C. **(b)** SEM image of two type (ii) GaS nanowires, grown with Ag catalysts. Note the catalyst particles at their tips. **(c)** Analysis of the spherical-cap shape of the solid catalyst. **(d)** TEM image of a type (ii) GaS nanowire, showing the diameters at the root (186 nm) and tip (371 nm). Estimating the shape of the molten catalyst as equal to that after crystallization (as shown in (b)), the tapered nanowire shape implies a 24-fold increase of the catalyst volume between the early (volume V_0) and final stages (volume 24 × V_0) of growth.

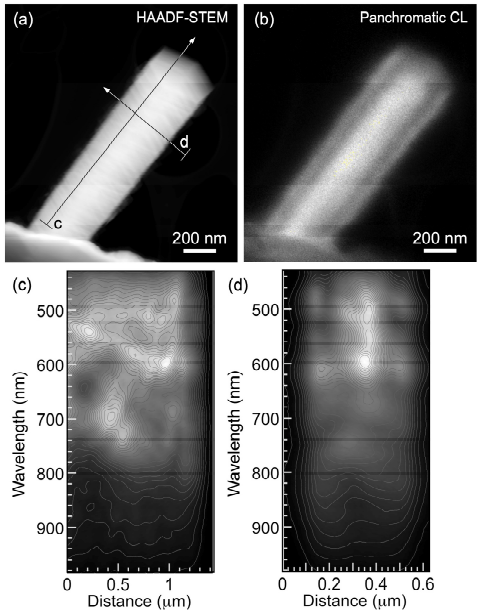

Figure S7. STEM-CL mapping and hyperspectral linescan of a thicker hexagonal GaS nanowire. **(a)** HAADF-STEM image of a thicker GaS nanowire with hexagonal cross-section. The tip with the VLS catalyst was likely broken off during dry-transfer to the TEM grid. **(b)** Panchromatic STEM-CL map of the nanowire shown in (a). **(c)** STEM spectral linescan along the line marked "c" in panel (a). **(d)** STEM spectral linescan across the wire (line "d" in panel (a)).

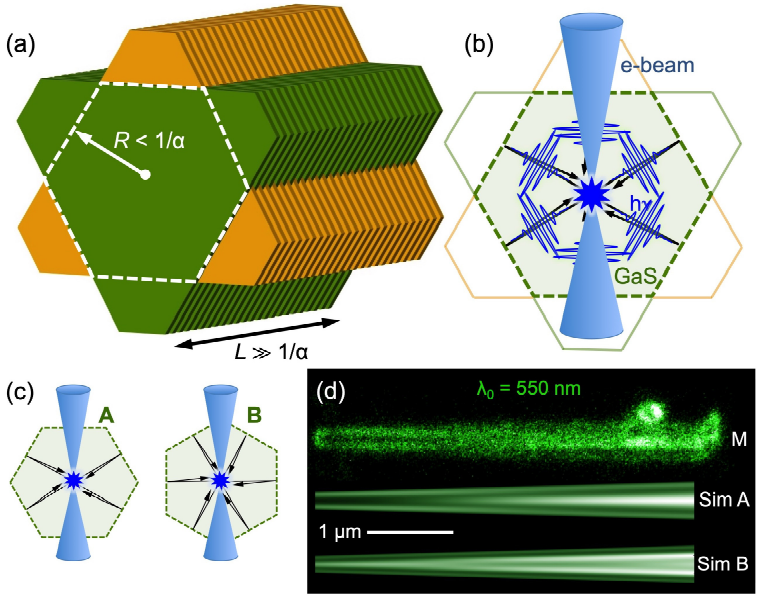

Figure S8. Interference of photonic waveguide modes launched by local electron beam excited luminescence. **(a)** Schematic of a type (ii) GaS nanowire with quasi-periodic twinning of truncated triangular few-layer flakes. Dashed line: outline of the hexagonal nanowire core. Note that the typical distances to the core surface (R ≤ 170 nm) are smaller than the absorption length (α^{-1}) of GaS, whereas the distance to the end facets L ≫ α^{-1}, so that reflection of waveguide photons by the side facets yields interference while the modes traveling along the wire axis do not interfere, except near the ends of the wire. **(b)** Schematic of the electron beam excitation, primary luminescence, and back-reflection by specular side facets. **(c)** Geometries of waveguide mode reflection for two different incidence directions of the electron beam. **(d)** Comparison of simulated interference patterns ('Sim A', 'Sim B', vacuum wavelength λ_0 = 550 nm) for geometries **A** and **B** shown in (c) with the experimentally measured intensity distribution ('M').

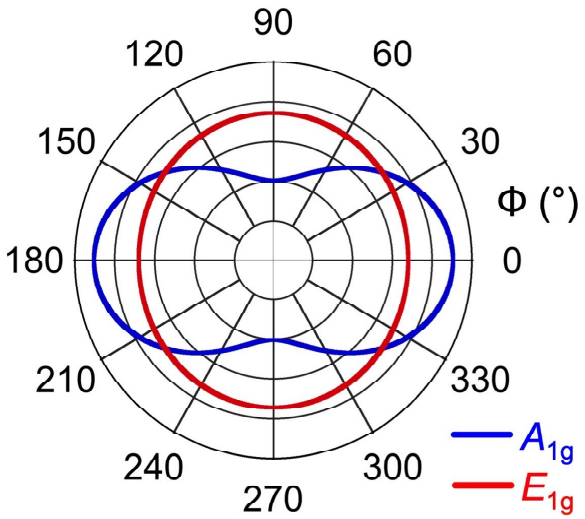

Figure S9. Predicted polarization-dependent Raman intensity for A_{1g} and E_{1g} modes of GaS. Colored curves illustrate equations (3) and (4) in Supporting Note 2, respectively, which describe the experimental situation of polarized incident light but collection of all scattered light independent of polarization.

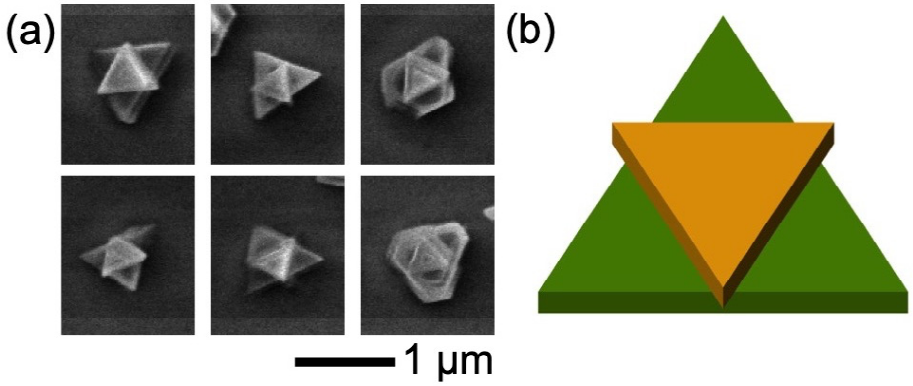

Figure S10. Twinning in planar GaS flakes. (a) Frequent twinning is observed in triangular and truncated triangular planar GaS flakes on the substrate surrounding fields of nanowires. **(b)** Schematic of the vertically stacked, twinned GaS flakes.

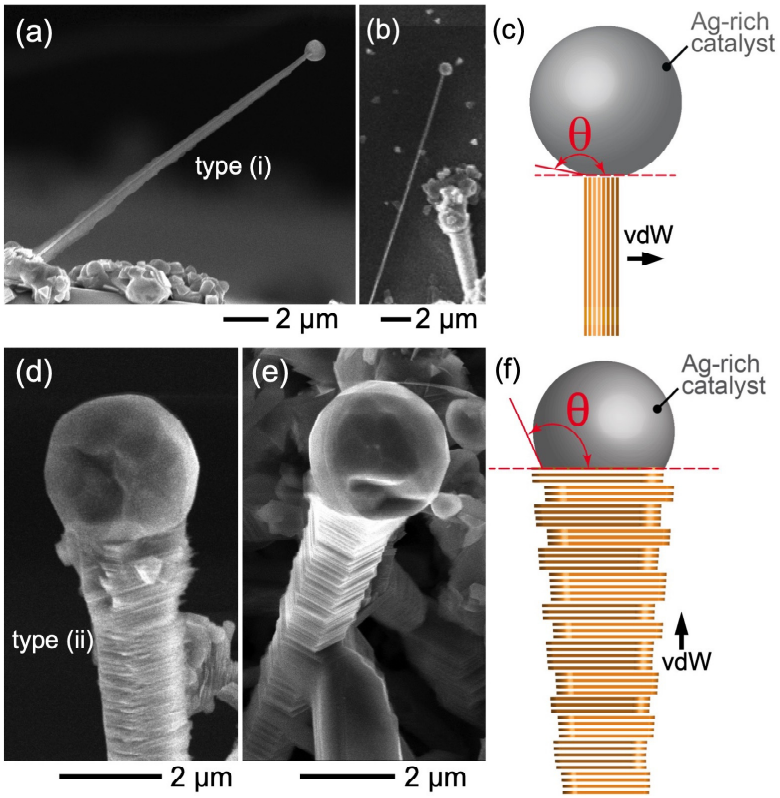

Figure S11. Differences in wetting of the Ag-rich VLS catalyst at the tips of type (i) and type (ii) GaS nanowires. (a) - (b) SEM image of a typical type (i) GaS nanowire. **(c)** Schematic illustration of the large contact angle (θ) of the Ag-rich catalyst at the type (i) nanowire tip, indicating non-wetting of the exposed GaS layer edges by the large catalyst drop. **(d) - (e)** SEM image of a typical type (ii) GaS nanowire. **(f)** Schematic illustration of the reduced contact angle (θ) of the Ag-rich catalyst at the type (ii) nanowire tip, indicating enhanced wetting of the GaS basal plane by the catalyst compared to type (i) nanowires.

Supporting Notes

Supporting Note 1: Volume and Composition Evolution of the Ag VLS catalyst

We used a geometrical analysis of tapered type (ii) wires to estimate the evolution of the Ag VLS catalyst during GaS nanowire growth. The spherical-cap shape of the catalyst is assumed constant during growth, and equal to the shape of the crystallized VLS tips observed by SEM (Figure 3 (a)). The corresponding catalyst drop volume is calculated as shown in Figure S6, for a base diameter of the spherical cap matching the local diameter of the tapered nanowire shown in Figure S6 (d). Using this procedure, we estimate that the volume of the VLS catalyst expands about 24-fold during the growth of the tapered type (ii) wire shown in Figure S6 (d).

This volume expansion can then be linked to a progressive increase in Ga content within the catalyst, assuming that the entire volume increase is due to retention of Ga in the drop (as described in the text). For this composition analysis, we assume that the initial composition is equal to that given by the Ag-Ga equilibrium phase diagram at the growth temperature T_s = 600°C, *i.e.*, about 30 at. % Ga (see Figure S6 (a)). The calculated volume increase then suggests a progressive increase in the Ga content to about 90 at. % Ga at the end of the growth of the nanowire shown in Figure S6 (d).

Supporting Note 2: Polarized Raman Spectroscopy

The analysis of the polarization-dependent Raman spectra follows the classification of the Raman-active modes of β-GaS by van der Ziel.[1] For the Raman-active modes analyzed here, E^1_{1g} and A^1_{1g}, the scattering tensor has the following non-vanishing components: A^1_{1g}: *zz*, *xx* + *yy*; and E^1_{1g}: *zx*, *yz*. Hence, the scattering tensors can be written as follows:

$$\mathrm{R}\left(A^1_{1g}\right) = \begin{pmatrix} a & 0 & 0 \\ 0 & a & 0 \\ 0 & 0 & b \end{pmatrix}; \quad \mathrm{R}_1\left(E^1_{1g}\right) = \begin{pmatrix} 0 & 0 & a \\ 0 & 0 & 0 \\ a & 0 & 0 \end{pmatrix}, \quad \mathrm{R}_2\left(E^1_{1g}\right) = \begin{pmatrix} 0 & 0 & 0 \\ 0 & 0 & b \\ 0 & b & 0 \end{pmatrix}.$$

For incident and scattered electric field (unit) vectors $\mathbf{e}_i$ and $\mathbf{e}_s$, respectively, the scattered intensity is calculated as: $$I = |\mathbf{e}_s^T \mathrm{R} \mathbf{e}_i|^2 \quad (1)$$

where the superscript T denotes the transposition from a column vector to a row vector.[2]

If, as in our experiments, no analyzer is placed in the path of the scattered light, this relation simplifies to: $$I = |\mathrm{R}\mathbf{e}_i|^2 \quad (2)$$

In our measurements on type (ii) GaS nanowires, the incident electric field vector lies in the (x, z) plane: $\mathbf{e}_i = \begin{pmatrix} \cos(\varphi) \\ 0 \\ \sin(\varphi) \end{pmatrix}$.

For the A^1_{1g} mode: $$I = a^2 \cos^2(\varphi) + b^2 \sin^2(\varphi) \quad (3)$$

For the E^1_{1g} mode: $$I = a^2 + \frac{b^2}{2}(1 - \cos(2\varphi)) \quad (4)$$

Figure S9 illustrates the expected two-fold symmetry of polar plots of Raman intensity as a function of polarization angle φ (compare also Fig. 5 of the main text):

Supporting Note 3: Confined Photonic Waveguide Modes in GaS Nanowires

A comparison of the measured monochromatic CL maps for three vacuum wavelengths λ_0 (450, 550, and 650 nm, shown in Figure 7 (f)) with simulations of the expected interference fringe pattern according to the model developed in Ref. [3] is used to establish interference of confined photonic waveguide modes as the origin of the observed intensity modulation in the experimental maps.

Waveguide modes are traveling photonic modes that propagate within the GaS nanowire (the 'waveguide'), with wavelength that is related to the vacuum wavelength λ_0 *via* $\lambda^{wg} = \lambda_0 \, n^{-1}$, where *n* denotes the (photon energy dependent) refractive index of GaS. We have shown previously that nanometer-scale locally excited luminescence in STEM-CL can launch such modes, which for photon energies in the transparency region can travel over significant distances in mesoscale structures. Specular surface facets, realized previously in mesoscale GeS prisms[3] and here in type (ii) GaS nanowires, internally reflect the propagating modes so that they can coherently add and generate an interference pattern. Within this framework, constructive interference is expected whenever the excitation (*i.e.*, the electron beam) is positioned at integer multiples of $\lambda^{wg}/2$ from the reflecting edge.

We have simulated the expected interference fringe pattern for the three vacuum wavelengths of our experimental monochromatic CL maps using the software package *Mathematica*. The excitation was placed at different distances from the (projected) edges of a type (ii) nanowire with the experimentally observed geometry (Figure 7 (a)). The overall intensity of the emitted light for each position of the exciting electron beam was computed by coherently adding the primary emission with beams internally reflected from the six sides of the hexagonal envelope

of the nanowire (*i.e.*, ignoring the corrugation of the protruding GaS flakes, see Figure S8 (b). The total intensity, with contributions from the entire thickness of the nanowire traversed by the electron beam, was then plotted for each wavelength as a false color density plot (Figure 7 (f)). We repeated this procedure for two orientations of the nanowire relative to the electron beam, namely 'edge up' (orientation **A** in Figure S8 (c)) and 'corner up' (orientation **B** in Figure S8 (c)). The observed fringe pattern fits closely with the experimentally observed intensity modulations at each wavelength if we assume the 'edge up' orientation (**A**) of the wire. The alternative 'corner up' orientation (**B**) produces a different fringe pattern that does not match the intensity distribution observed experimentally (Figure S8 (d)).

Supporting References

1. van der Ziel, J. P.; Meixner, A. E.; Kasper, H. M. Raman Scattering from β-GaS. *Solid State Commun.* **1973**, *12*, 1213-1215.
2. Saito, R.; Tatsumi, Y.; Huang, S.; Ling, X.; Dresselhaus, M. S. Raman Spectroscopy of Transition Metal Dichalcogenides. *J. Phys.: Condens. Matter* **2016**, *28*, 353002.
3. Sutter, P.; Argyropoulos, C.; Sutter, E. Germanium Sulfide Nano-Optics Probed by STEM-Cathodoluminescence Spectroscopy. *Nano Lett.* **2018**, *18*, 4576-4583.